Correspondence to:
M. Chen,
mingli.chen@polyu.edu.hk

Leader Charges, Currents, Ambient Electric Fields, and Space Charges Along Downward Positive Leader Paths Retrieved From Ground Measurements in Metropolis

Yan Gao[1,2] , Mingli Chen[1] , Weitao Lyu[3,4] , Qi Qi[3], Zilong Qin[1,2] , Ya-ping Du[1], and Yijun Zhang[5]

[1]Department of Building Service Engineering, The Hong Kong Polytechnic University, Hong Kong, [2]Guangdong-Hong Kong-Macao Greater Bay Area Weather Research Center for Monitoring Warning and Forecasting (Shenzhen Institute of Meteorological Innovation), Shenzhen, China, [3]State Key Laboratory of Severe Weather, Chinese Academy of Meteorological Sciences, Beijing, China, [4]Laboratory of Lightning Physics and Protection Engineering, Chinese Academy of Meteorological Sciences, Beijing, China, [5]Institute of Atmospheric Sciences, Fudan University, Shanghai, China

Abstract An approach for retrieving the leader channel charge density, leader current, ambient electric field, and space charge along a leader channel path from ground observations with a complicated ground condition was presented. With this approach, properties of two downward positive leaders (DPL1 and DPL2) struck at high-rise buildings were studied based on electric and optical measurements made on the roof of a 100 m high building in Guangzhou, China. It shows that the leader-produced electric field on the roof of the 100 m high building was about 4 times of that on flat ground. The 2-D speed for both leaders showed a general increasing trend as the leader going down, in the range of 1.8 to 32.3×10^5 and 1.7 to 46.9×10^5 m/s, respectively. The channel line charge density for both leaders showed firstly a sharp increasing trend and then a decreasing trend as the leader going down, in the range of 0.4 to 8.6 and 0.4 to 15.2 mC/m, respectively. The current of the two leaders varied in the range of 0.7 to 5.4 and 0.7 to 4.6 kA, respectively. The ambient electric field (downward is positive) for both leaders showed an alternating polarity along the leader path, in the range of -120 to $+176$ and -250 to $+180$ kV/m, respectively. The space charge for both leaders showed also an alternating polarity along the leader path, in the range of -12.3 to $+4.2$ and -13.9 to $+7.8$ nC/m^3, respectively, which may reflect the in-cloud electric structure and the corona charge distribution between the cloud and ground.

1. Introduction

A positive lightning discharge is defined as a flash transporting positive charge from cloud to ground, and the one that is started with a downward positive leader (DPL) is called a downward positive discharge. Statistics show that less than 10% of global cloud-to-ground discharge is positive (Rakov & Uman, 2005). Due to the high current and large charge transferring to ground, positive lightning often causes more severe damage to objects and systems than negative one (Idone et al., 1984; Le Boulch & Plantier, 1990; Nakahori et al., 1982). Study of the property of DPL is critical for the protection of objects and systems against positive lightning.

It is generally thought that a continuously moving positive leader is mainly comprised of leader tip, leader channel, and streamer zone (Gorin et al., 1976). The moving speed of a positive leader may increase from 10^4 to 10^6 m/s with the average being about 10^5 m/s as it advances (Berger, 1975; Gao et al., 2014, 2020; Idone, 1992; Kong et al., 2008; Rakov, 1999; Saba et al., 2008; Wada et al., 2003).

Besides the speed, the leader channel charge density is another important parameter for understanding the mechanism of initiation and propagation of a leader. However, due to lack of methods to measure the channel charge directly, there is little data on it. A traditional method for remote sensing of the leader parameters in nature lightning is to estimate the leader charge and current from the leader electric and magnetic field measurements based on reasonable electro-static and magneto-static approximations (e.g., Krehbiel, 1981; Krider et al., 1977; Proctor, 1991, 1997; Thomson et al., 1985; Thottappillil et al., 1997). But most results with this method are on the average leader current and charge density along negative leader channels. Alternatively, the leader current and speed measured simultaneously could be

used to estimate the line charge density of an upward positive leader (UPL), which shares some characteristics with DPL. For example, from the ratio between the leader current and its speed, Lalande et al. (2002) estimated the line charge density of UPL as about 500 μC/m during the late stage of the leader propagation.

Chen, Zheng, et al. (2013) proposed an approach to estimate the leader charge density and leader current from close-distant electric field observation and high-speed camera imaging of the leader channel made on flat ground. With that approach, they estimated the line charge densities and currents of two UPLs during rocket-triggered lightning experiments, which were well consistent with the currents measured at the channel base. The average values of leader charge densities were 154.8 and 62.2 μC/m, respectively. The similar method was used to calculate the line charge density of two downward negative leaders to flat ground and the range of the line charge density was from −20 to −330 μC/m (Shen et al., 2018). The average line charge density obtained for positive leaders in long gap experiment ranged in 20 to 50 μC/m (Les Renardieres Group, 1977).

Besides experiments, there are many simulative studies of the positive leader with different models (Becerra & Cooray, 2006; Chan et al., 2018; Dellera & Garbagnati, 1990; Mazur, 1989; Rubenstein et al., 1995). In those models, the main leader properties including the leader channel line charge density, leader current, leader channel potential gradient, and propagation speed can be self-consistently simulated.

In fact, the leader channel charge density is highly related to the preexisting ambient electric field profile along the leader channel path. To understand the mechanism of leader initiation and propagation, it is crucial to get knowing the ambient electric field profile associated with the event. Some balloon measurements were done to record the corona current and vertical electric field under thunderstorms, from which the average charge densities inside the thunderstorm, and hence, the electrical structure of the thunderstorm were inferred (Byrne et al., 1983; Marshall & Rust, 1991, 1993; Schuur et al., 1991; Shepherd et al., 1996). And some cloud charge models were built to present the relationships between the cloud charge, potential, ambient electric field, and the leader channel parameters (Bazelyan & Raizer, 2000; Chen, Gou, & Du, 2013; Iudin et al., 2017; Mazur & Ruhnke, 1998; Xu & Chen, 2013).

In this study, an improved approach for estimating the leader channel charge density and current as well as the associated ambient electric field and space charge of DPLs struck at high-rise buildings from electric field and high-speed camera observations made on the roof of a building in a metropolis is proposed and practiced. Compared with previous studies, this approach can be used to analyze lightning discharges occurring above a complicated earth boundary. Details of the approach and its application results are presented in following sections.

2. Lightning Data Acquisition

To study the characteristics of lightning discharges attaching to high-rise buildings, the Tall-Object Lightning Observatory in Guangzhou (TOLOG) has been established by Lu et al. (2013). The main observation station was located on the roof of a 100 m high building that belongs to the Guangdong Meteorological Bureau.

At the main observation station, two Lightning Attachment Process Optical Observation Systems (LAPOSs) (Wang et al., 2011) were installed to observe the lightning events in the field of view. In 2015, several Photron Fastcam high-speed cameras with different configurations were installed at the main station to capture the lightning channel images. In this study, all high-speed images analyzed were obtained by one of these high-speed cameras, labeled as HC-1. The HC-1 had a monochrome sensor with a focal length of lens of 14 mm, operated at a rate of 10,000 frames per second with an exposure time of 99.754 μs per frame, a recording time of 50 ms per event and a 20% pretrigger time.

Besides, two slow antennas (SA1 and SA2) with different measurement ranges were installed at the main station to measure the electric field changes during lightning flashes. Due to the small measurement range (±100 kV/m) of SA1, the E field data observed by SA1 were saturated in the cases analyzed. Therefore, all E field data used in this study were obtained by SA2, which had a measurement range of ±200 kV/m with a bandwidth of 0.03 Hz to 2 MHz and a time constant of 6 s. The output of SA2 was digitized and logged by
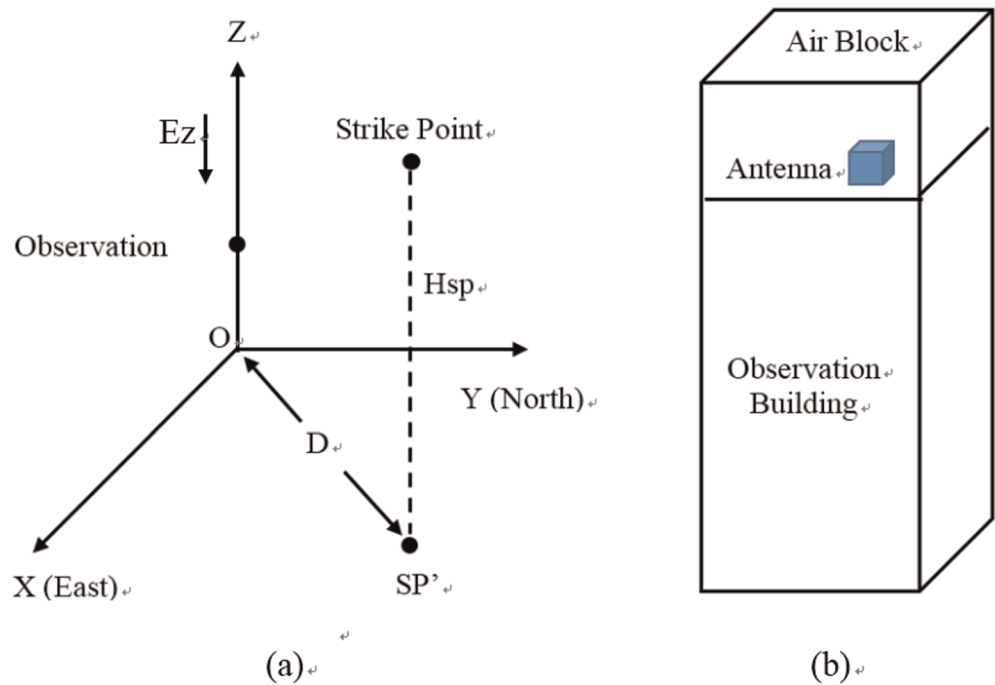
Figure 1. (a) Setup of the 3-D coordinate system for this study: The origin O and SP′ are the projection points of the observation site and the lightning strike point on ground, respectively. H_{ob} and H_{sp} are the heights of the observation site and the lightning strike point, respectively. D is the horizontal distance from the observation site to the lightning strike point. (b) Setup of the simulation space around the observation site: The sizes of the observation building, the additional air block and the antenna block are 20 m × 20 m × 100 m, 20 m × 20 m × 20 m and 0.5 m × 0.5 m × 0.5 m, respectively, and the corresponding mesh element sizes are 10, 1, and 0.1 m, respectively. The positive direction for E field E_z is downward in this study.

a DL850 data recorder with a digitalizing rate of 10 megasamples per second, a recording time of 1 s and a 10% pretrigger time. One channel of the LAPOS was used as the trigger source for both HC-1 and SA2, and SA2 could also be triggered by itself.

3. Data Analysis Method

3.1. Setup of Coordinates and Simulation Space

First, we need to define a 3-D coordinate system that is used to retrieve the line charge density of a leader. Figure 1a is an illustration of the 3-D coordinate system we used. The origin of the 3-D coordinate system represents the projection point of the observation site on ground. The direction of X axis is to the east, the direction of Y axis is to the north, and the direction of Z axis is straight up. H_{ob} presents the height of the observation site on the roof of a building, that is, the coordinate of the observation site is (0, 0, H_{ob}). H_{sp} represents the height of the strike point of a lightning flash at a building and SP′ is the projection point of the strike point on ground. The horizontal distance between the observation site and the strike point is D.

Second, to simulate the leader-produced electric field at the observation site, the subroutine for electrostatics of the computer code COMSOL is adopted. Based on the strike points of the two DPLs to be analyzed and the detection range of the instrument, a 10 km × 10 km × 10 km cube around the TOLOG observation station is selected as the simulation space. The upper half of the simulation space is above the ground, and the lower half space is chosen as the soil layer under the ground. By using Google Earth (2015), we find that there were 22 high-rise buildings (including the observation building), of which the heights were higher than 100 m, within the simulation space. These 22 tall buildings are digitized as 20 m × 20 m × H (H represents the height of each tall object) block above the ground and the rest is simplified as flat ground. There is also a 0.5 m × 0.5 m × 0.5 m block around the slow antenna (SA2) installed on the roof of the observation building. In the simulation model, the mesh element size for the 22 building blocks is 10 m and that for the SA2 block is 0.1 m. To improve the accuracy of the simulated electric field at SA2, an additional 20 m × 20 m × 20 m air

block, of which the mesh element size is 1 m, is added on the roof of the observation building. The additional air block contains the antenna block, as shown in Figure 1b. The mesh element size of the rest space in the simulation model ranges from 540 to 3,000 m, determined by COMSOL itself as the normal standard.

3.2. Basic Theory

In this section, some basic theories used in analyzing the observation data are introduced.

3.2.1. Relationship Between Electric Field Change and Leader Charge Density

For a lightning leader, the transferred line charge density along the leader channel is defined as $\lambda = dQ/dl$, where dQ is the charge transferred from the cloud into a channel segment of length dl. In previous studies (Chen, Zheng, et al., 2013; Shen et al., 2018), a basic assumption was that charges being added to the leader tip were transferred directly from the electric source in cloud/ground and charges along the established channel behind the leader tip kept unchanged as the leader developed, which is adopted in this study too. For the electric field measurement at TOLOG, because the observation site is several kilometers away from the cloud and the lightning channel, the electric charge source in cloud can be simplified as a point charge. According to the principle of charge conservation, when a positive unit charge is transported directly from the electric charge source in cloud to the leader tip, a negative unit charge is left in the cloud. As a result, the transferred line charge density (λ) at the leader tip is related to the leader current (I) and the leader tip moving speed (v) as

$$\lambda = \frac{dQ}{dl} = \frac{Idt}{vdt} = \frac{I}{v}. \tag{1}$$

In practice, it is impossible to measure the current along a downward leader channel directly and, hence, cannot get the leader line charge density from the leader current measurement. On the other hand, based on the study by Chen, Zheng, et al. (2013), the charges transported from the charge source to a new leader channel segment above a flat ground can be estimated from the electric field measurement on ground, which is much more achievable than the current measurement. However, for a lightning leader occurring in metropolis with crowded buildings, the Earth boundary condition around the observation site is complicated, making the electric field measurement different from that above a flat ground.

Taking account of the influence of the complicated ground condition, the vertical electric field change dEz_{tip} at the observation site H_{ob} in height, produced by the charge at the leader tip with a line charge density λ and a small segment length dl centered at H_{tip} in height and D_{tip} in horizontal distance to the observation site, can be written as

$$dEz_{tip} = \frac{k_1(l) \times dQ_{tip}(H_{tip} - H_{ob})}{4\pi\varepsilon_0 \left[D_{tip}^2 + (H_{tip} - H_{ob})^2\right]^{\frac{3}{2}}} = \frac{k_1(l) \times \lambda dl(H_{tip} - H_{ob})}{4\pi\varepsilon_0 \left[D_{tip}^2 + (H_{tip} - H_{ob})^2\right]^{\frac{3}{2}}}, \tag{2}$$

where $k_1(l)$ is a coefficient depending on the leader tip position (l) and the earth boundary and downward direction of the electric field is positive.

As dQ_{tip} is transported from the charge source in cloud to the leader tip, the same amount of opposite charges dQ_{source} is left in cloud. Assume the height of the charge source in cloud is H_{source} and its horizontal distance to the observation site is D_{source}, the vertical electric field change dEz_{source}, produced by the point charge dQ_{source} is

$$dEz_{source} = \frac{k_2(l) \times dQ_{source}(H_{source} - H_{ob})}{4\pi\varepsilon_0 \left[D_{source}^2 + (H_{source} - H_{ob})^2\right]^{\frac{3}{2}}} = \frac{-k_2(l) \times \lambda dl(H_{source} - H_{ob})}{4\pi\varepsilon_0 \left[D_{source}^2 + (H_{source} - H_{ob})^2\right]^{\frac{3}{2}}}, \tag{3}$$

where $k_2(l)$ is another coefficient depending on the dQ_{source} position (l) and the earth boundary.

In real cases, both dQ_{tip} and dQ_{source} influence the observed electric field changes. The total observed vertical electric field change as a function of the leader tip position (the time) at the observation site is

$$dE_{ob} = dEz_{tip} + dEz_{source} = \frac{\lambda dl}{4\pi\varepsilon_0} \left\{ \frac{k_1(l) \times (H_{tip} - H_{ob})}{\left[D_{tip}^2 + (H_{tip} - H_{ob})^2\right]^{\frac{3}{2}}} - \frac{k_2(l) \times (H_{source} - H_{ob})}{\left[D_{source}^2 + (H_{source} - H_{ob})^2\right]^{\frac{3}{2}}} \right\}. \tag{4}$$

To get the transferred line charge density at the leader tip, a simulation model has been built. In the model, suppose that a unit positive charge is transferred from cloud to the leader tip position in a unit channel length, the vertical electric field change due to this charge, dE_{si}, at the observation site is

$$dE_{si}/dl = \frac{\lambda_0}{4\pi\varepsilon_0} \left\{ \frac{k_1(l) \times (H_{tip} - H_{ob})}{\left[D_{tip}^2 + (H_{tip} - H_{ob})^2\right]^{\frac{3}{2}}} - \frac{k_2(l) \times (H_{source} - H_{ob})}{\left[D_{source}^2 + (H_{source} - H_{ob})^2\right]^{\frac{3}{2}}} \right\}, \tag{5}$$

where λ_0 is the unit line charge density and dE_{si}/dl can be calculated through the simulation subroutine. As such, the transferred leader line charge density as a function of the leader tip position can then be obtained by comparing the observed electric change with the simulated one as

$$\lambda(l) = \left(\frac{dE_{ob}}{dl}\right) / \left(\frac{dE_{si}}{dl}\right) \cdot \lambda_0. \tag{6}$$

And the corresponding leader current as a function of the leader tip position can be estimated as

$$I(l) = \lambda(l) \cdot v(I) \tag{7}$$

3.2.2. Relations of Leader Charge Density, Ambient Electric Field, and Space Charge

Physically, it is the ambient electric field that determines the line charge density along the leader channel. When a cloud is charged above a flat ground, an ambient electric field will be established between the cloud and ground. For simplification, assuming the potential, $\varphi(z)$, between the cloud and ground is horizontally homogeneous, the vertical electric field, $Ez(z)$, along a vertical path between the cloud and ground is given by

$$\frac{\partial\varphi(z)}{\partial z} = Ez(z), \tag{8}$$

where the downward direction of $Ez(z)$ is defined as the positive, which means a positive charge overhead produces a positive electric field on ground.

If there are space charges that are horizontal homogeneously distributed around a vertical path between the cloud and ground, the volume density of the space charge, $\rho(z)$, along the vertical path is given by

$$\text{div}Ez(z) = \frac{\partial Ez(z)}{\partial z} = -\frac{\rho(z)}{\varepsilon_0} \tag{9}$$

The space charge refers to those charges previously existing in and out the cloud before the leader occurrence. It is the space charge that determines the ambient electric field which governs the leader process followed. To study the profiles of the ambient electric field associated with the development of a downward leader process, the above equations should be further modified. Many studies show that a leader channel is composed of a core surrounded by a corona sheath. The leader core is well ionized and highly conductive with a radius no more than a centimeter, while the corona sheath is highly charged with a radius up to tens of meters. When the leader charge is deposited on the core, the charge creates a strong radial electric field that pushes the charge away from the core, forming the corona sheath (Maslowski & Rakov, 2006).

Figure 2a shows a cylindrically symmetric structure of a DPL channel. As the leader propagates downward from cloud, the potential along the leader channel core at a given time, t, is given by

$$\varphi_{core}(z, t) = \varphi_{cloud} - E_L(t) \times (z_{cloud} - z), \tag{10}$$

where φ_{cloud} and z_{cloud} are the potential and height of the leader origin in the cloud, respectively, and $E_L(t)$ is the longitudinal electric field along the channel core (Bazelyan & Raizer, 2000; Chen, Gou, & Du, 2013). Since $E_L(t)$ is usually small, it will be neglected in calculations in this study.
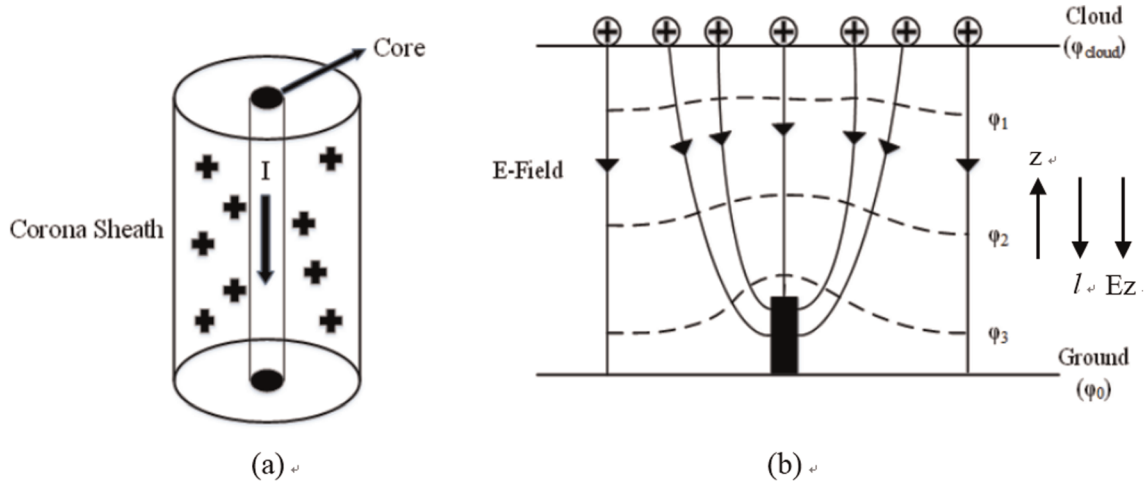
Figure 2. (a) A schematic of the channel structure of a downward positive leader. (b) A schematic of the ambient potential and electric field profile above a high-rise building under a thunderstorm, where φ_{cloud} and φ_0 are the cloud and ground potentials, respectively; the solid lines represent the ambient electric field and the dashed lines represent the equipotential plane. The three arrows in the right represent the positive directions of z, l, and Ez, respectively.

The charge transferred from the cloud to the leader channel (λ) is mainly deposited in the corona sheath, together with the preexisting space charge (ρ) there to balance the potential difference between the leader core and the ambient. Assuming the preexisting space charge (ρ) is horizontally uniform (the ambient electric field is with only vertical component), then the transferred line charge density (λ) can be related to the potential difference between the leader core and the ambient as

$$\Delta\varphi(z) = \varphi_{core}(z) - \varphi_{ambient}(z) = \int_0^\infty E(r) \cdot dr \approx \frac{\lambda(z)}{2\pi\varepsilon_0}. \tag{11}$$

The ambient electrical field along the leader channel path is given by

$$Ez_{ambient}(z) = \frac{\partial\varphi_{ambient}(z)}{\partial z} = E_L - \frac{1}{2\pi\varepsilon_0}\frac{\partial\lambda(z)}{\partial z} \tag{12}$$

And the volume density of space charges along the leader channel path is given by

$$\rho(z) = -\varepsilon_0\frac{\partial Ez_{ambient}(z)}{\partial z}. \tag{13}$$

On the other hand, by assuming that the transferred line charge density (λ) is all deposited within the corona sheath (in fact, some of transferred charge is out of the corona sheath as shown by Equation 11, this is one limitation of definition of the corona sheath radius), then according to Gauss's Law, the net line charge density (λ_n) in the corona sheath is related to the radial electrical field (E_r) at the cylindrical surface of the equivalent corona sheath radius (R_s) as

$$\oint_S E(S) \cdot dS = 2\pi R_s(z)E_r = \frac{\lambda_n(z)}{\varepsilon_0}, \text{ and } \lambda_n(z) = \lambda(z) + \pi R_s^2\rho(z) = 2\pi\varepsilon_0 E_r R_s(z) \tag{14}$$

The physical solution of R_s for a positive leader ($E_r > 0$, $R_s > 0$, $\lambda_n > 0$, and $\lambda > 0$) is

$$R_s(z) = \begin{cases} \dfrac{\varepsilon_0 E_r\left[1 - \sqrt{1 - \dfrac{\rho(z)\lambda(z)}{\pi(\varepsilon_0 E_r)^2}}\right]}{\rho(z)}, & \rho(z) \neq 0 \\[20pt] \dfrac{\lambda(z)}{2\pi\varepsilon_0 E_r}, & \rho(z) = 0 \end{cases} \tag{15}$$

where $\lambda(z)$ is the leader line charge density transferred from the cloud into the leader corona sheath in the leader process, $\rho(z)$ the volume space charge density existed in the corona sheath before the leader process, $\lambda_n(z)$ the net leader line charge density deposited in the corona sheath in the leader process, $R_s(z)$ the

equivalent radius of the corona sheath, S the cylindrical surface area with the radius R_s and a length of 1 m, and E_r is the radial electrical field at the corona sheath surface which is more or less equal to the critical E field required to support a positive streamer propagation (Chan et al., 2018; Maslowski & Rakov, 2006, 2013; Xu & Chen, 2013).

In this study, the Earth boundary is not flat but contains 22 high-rise buildings, making the profiles of ambient potential and electric field different from that above a flat ground.

Figure 2b is a schematic of the ambient potential and electric field profiles around a building under a thunderstorm, where the potential of the cloud and earth boundary is φ_{cloud} and φ_0, respectively. The solid lines represent the ambient electric fields, while the dashed lines represent the equipotential planes. If there is a space charge distributed in the space, it also affects the ambient potential and electric field.

When a DPL propagates downward, we suppose that the ambient potential gradient along its path is the maximum and the ambient potential is normal homogeneous along its path. Then the transferred leader line charge density along the leader channel can be related to the potential difference between the leader core and the ambient as

$$\Delta\varphi(l) = \varphi_{core}(l) - \varphi_{ambient}(l) = \frac{\lambda(l)}{2\pi\varepsilon_0},$$ (16)

where l represents the path along the DPL channel which starts in cloud and points downward. That is, "l" is equivalent to "$z_{cloud} - z$" and "dl" is equivalent to "$-dz$", comparing to Equations 10–15. As a result, the ambient longitudinal electric field along the leader path can be estimated as

$$E_{ambient}(l) = -\frac{\partial\varphi_{ambient}(l)}{\partial l} = E_L + \frac{1}{2\pi\varepsilon_0}\frac{\partial\lambda(l)}{\partial l}.$$ (17)

And the volume density of the space charges along the leader channel path can be estimated as

$$\rho(l) = \varepsilon_0\frac{\partial E_{ambient}(l)}{\partial l}.$$ (18)

3.3. Practical Algorithm

Step 1. For a given DPL, by using high-speed camera images with the 2-D approximation method in Chen et al. (1999), the 2-D leader propagation channel trace, l, and the 2-D propagation speed, $v(t)$, can be estimated. According to the lightning striking point and the 3-D coordinate system mentioned in section 3.1, the 2-D leader channel trace can be transformed to a 3-D coordinate sequence as $l(x, y, z)$.

Step 2. Since both HC-1 and SA2 are triggered by the same channel of the LAPOS and synchronized with the same GPS timer, the observed electric field as a function of time can be transformed to one as a function of the leader tip position via the leader speed. With the 2-D leader speed, $v(t)$, the time derivative of the vertical electric field, $dE_{ob}(t)/dt$, obtained with SA2 at the observation site can be transformed to the channel length derivative of the electric field change, $dE_{ob}(l)/dl$, as

$$\frac{dE_{ob}(l)}{dl} = \frac{dE_{ob}(t)}{dt}\cdot\frac{dt}{dl} = \frac{dE_{ob}(t)}{dt}\cdot\frac{1}{v(t)}.$$ (19)

Step 3. In the COMSOL model, the whole simulation space, including the 22 buildings mentioned in section 3.1 (Condition 4), is adequately digitalized. Since the electric field observation site is several kilometers away from the DPL, the leader channel can be simplified as a thin wire. The source height can be fixed at a reasonable value, say 5,000 m high above ground in this study. Suppose that as the leader propagates every 1 m along the leader channel, $l(x, y, z)$, there is a unit positive charge transported from the cloud to the leader tip with a unit negative charge left in the cloud. The vertical
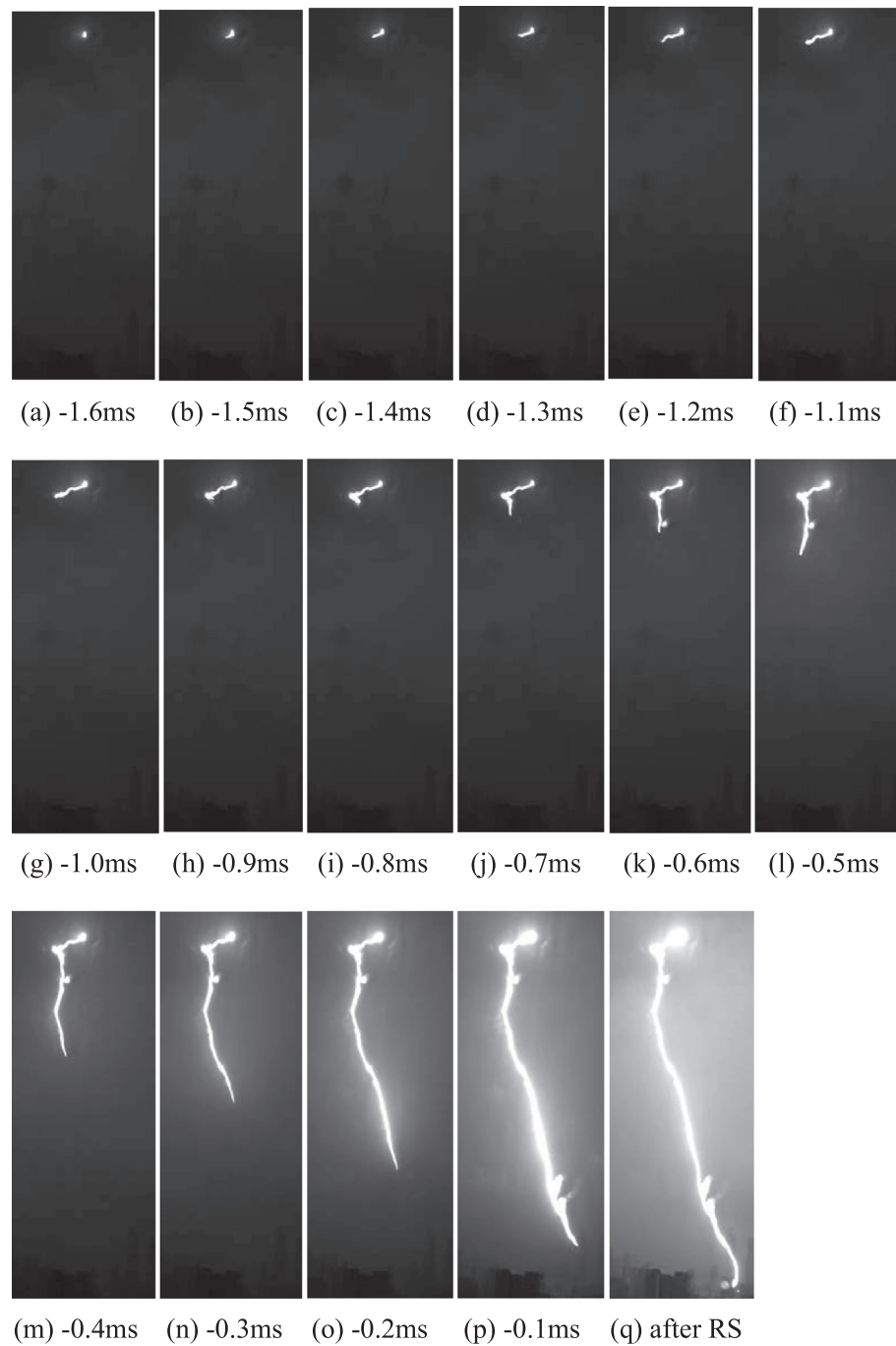
Figure 3. High-speed images of DPL1. Time 0 is set at the beginning of the return stroke, (a–p) captured before the return stoke and (q) after the return stroke. The extent of view of each panel is from about 100 to 2,000 m height above ground.

electric field change produced by this unit charge (λ_0) and its induced charge on the earth boundary at the observation site, $dE_{si}(l)/dl$, as a function of the leader tip position can be simulated with the COMSOL model.

Step 4. The actual transferred leader line charge density along the leader channel, $\lambda(l)$, can then be obtained by the ratio of the observed electric field change, $dE_{ob}(l)/dl$, to the simulated unit charge-produced electric field change, $dE_{si}(l)/dl$, as shown by Equation 6. The leader current is then given by
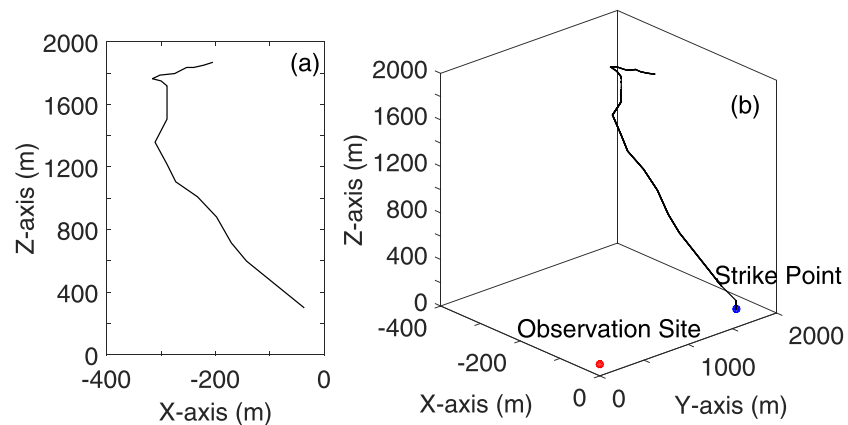
Figure 4. The 2-D channel rebuilt from HC-1 (a) and the channel in the 3-D coordinates in the simulation model (b) for DPL1. The horizontal distance from the observation site to the strike point is about 1,550 m.

Equation 7. In general, the resulted $\lambda(l)$ will fluctuate significantly. This is because the resolution of $v(t)$ and dE/dt is at channel segment level of about 20 m or something like that, which does not match with the element level (1 m) in the COMSOL model. To eliminate such an error, the transferred leader channel line charge density $\lambda(l)$ estimated should be integrated and averaged over a certain channel length, say 20 m, before it can be used for estimating the ambient electric field.

Step 5. To estimate the ambient electric field and the space charge along the leader channel path, the core-corona-sheath structure of the leader channel should be adopted. With the transferred leader line charge density, $\lambda(l)$, the ambient electric field, $E_{ambient}(l)$, along the leader channel path can then be estimated with Equation 17. Since the leader channel longitudinal electric field, $E_L(l)$, is generally very small, it could be ignored in estimating $E_{ambient}(l)$. Similarly, to reduce the error due to the fluctuation of the estimated ambient electric field profile, the ambient electric field should be averaged for each 20 m over a certain channel length, say 60 m, before it can be used for estimating the volume density of space charge along the leader path with Equation 18.

4. Results and Analysis

In this section, properties of two DPLs struck at two tall buildings in Guangzhou are investigated with the approach presented above. The properties studied include the leader channel charge density, the leader current, and the associated ambient electric field and space charge density along the leader channel path.

4.1. Case 1 (DPL1)

This was a DPL1 started cloud-to-ground lightning flash occurred at 15:53:58 LT on 13 August of 2015. Only one return stroke was reported by local lightning location network with a peak current of +145 kA.

Figure 3 shows a series of high-speed images of DPL1 captured by HC-1 at the observation site. The strike point of DPL1 was on the top of a tall building called Starry Winking. The height of this building was 156 m, and the horizontal distance from it to the observation site was about 1,550 m. As can be seen from the figure, there are several bright protrusion parts along the leader channel. These might be some loops related to 3-D channel structure or some spark discharges due to local space charge pockets. Figures 4a and 4b show the rebuilt 2-D and 3-D channels of DPL1, respectively.

From the 2-D channel images of DPL1, the 2-D propagation speed of DPL1 is estimated, as shown in Figure 5a, where the blue line represents the raw data and the red line represents the ninth-order polynomial curve-fitted speed. As can be seen from the figure, the leader speed increases from about 1.8×10^5 to 3.22×10^6 m/s as the leader goes downward from about 1,860 m high to 300 m high above the ground with a mean value of 1.11×10^6 m/s. Limited to the sampling rate and space resolution of HC-1, the 2-D speed estimated from the camera images is discontinuous, which may cause errors in the following calculation.
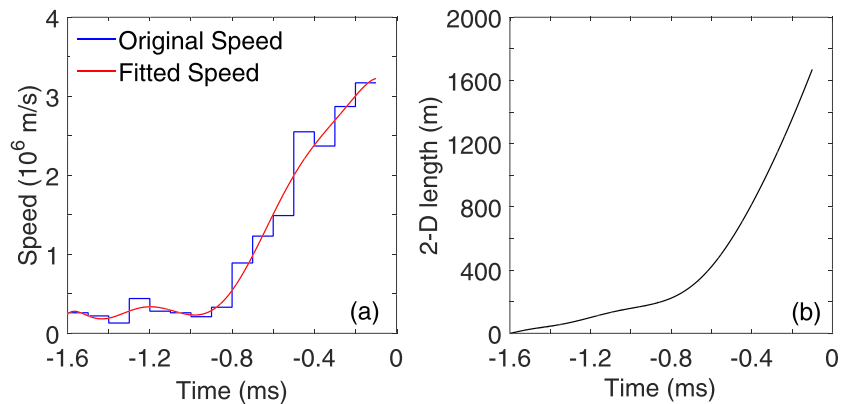
Figure 5. (a) The 2-D speed versus time for DPL1, the blue and red lines represent the observed and the curve-fitted speeds, respectively; (b) the 2-D channel length versus time for DPL1, which is obtained from the curve-fitted speed in (a); time 0 is set at the beginning of the return stroke.

To eliminate such errors in the following calculation, the 2-D speed is curve fitted. With the fitted speed curve, the 2-D channel length of DPL1 versus time is estimated, as shown in Figure 5b.

Shown in Figure 6a is the electric field changes observed for DPL1, where the two vertical dashed lines indicate the start and end time of the calculation for the leader. Time 0 is set at the beginning of the return stroke, which is synchronized with the high-speed images. In practice, the time derivatives of the electric field change is very sensitive to noises arisen during the experiment. In order to minimize this kind of influence, the electric field waveform originally sampled with a time interval of 0.1 μs (sampling rate 10 MHz) is processed by the method of five points moving average to filter out noises with higher frequencies. With the processed electric field changes, the time derivatives, dE_{ob}/dt, and, hence, the channel length-derivatives of the electric field, dE_{ob}/dl, are obtained with Equation 19, as shown in Figure 6b.

As Step 3 in section 3.3, to simulate the electric field change rate, dE_{si}/dl, we assume that there is line charge density of 1 C/m along the DPL1 channel, that is, when DPL1 extends downward every 1 m, 1 C positive charge is transferred from the cloud source to the tip of the leader with 1 C negative charge left in the cloud source. To estimate how the 22 buildings affect the electric field change produced by the leader at the observation site, four different kinds of ground conditions are adopted in the simulation: Condition 1—a flat ground, Condition 2—only the observation building on ground, Condition 3—both the observation building and the building being struck by DPL1 on ground, and Condition 4—all the 22 buildings on ground. In
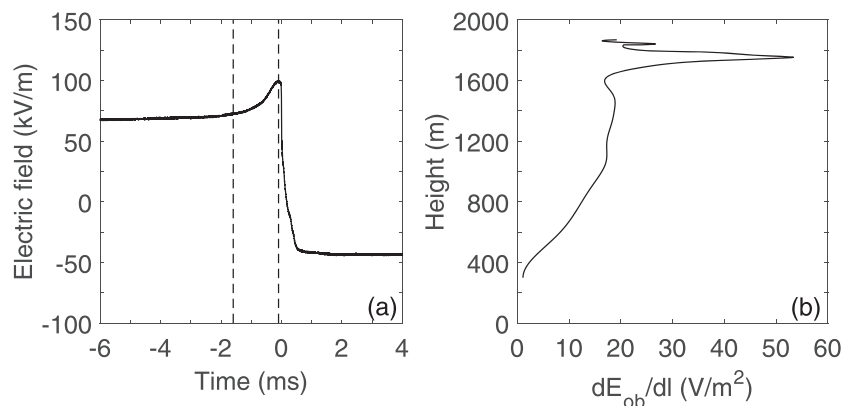
Figure 6. (a) The electric field changes produced by DPL1, the two vertical dashed lines indicate the start and end time of the calculation; (b) the channel length derivatives of the electric field changes, dE_{ob}/dl, versus height, calculated from the electric field shown in (a) and the curve-fitted speed shown in Figure 5a for DPL1.
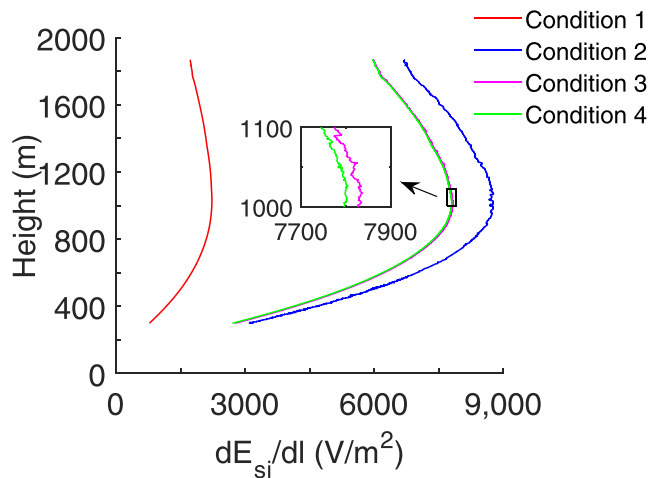
Figure 7. The simulated channel length derivatives of the electric field change, dE_{si}/dl, versus height along the DPL1 channel with a unit (1 C/m) line charge density. Four curves represent the results under four ground conditions: red curve for Condition 1—a flat ground, blue curve for Condition 2—only the observation building on ground, purple curve for Condition 3—both the observation building and the building being struck by DPL1 on ground, green curve for Condition 4—all the 22 buildings on ground. The subpanel is to show the difference between purple and green curves at the height of 1,000 to 1,100 m for easy reading.

Condition 1, due to lack of the observation building, the new observation point is set at the projection point of the original observation site on ground.

The simulated results with the four ground conditions are shown in Figure 7, where the red, blue, purple, and green lines represent the dE_{si}/dl simulated with Conditions 1 to 4, respectively. Since the simulated dE_{si}/dl for Conditions 3 and 4 are too close to each other, a subpanel for them is presented in the figure to show their difference at the height of 1,000 to 1,100 m.

As can be seen from Figure 7, the ratio of dE_{si} with (Condition 4) and without (Condition 1) the 22 buildings on ground is about 3.5, indicating that the 22 buildings together have a great influence on the electric field measurement at the observation site during DPL1. Particularly, the ratio of dE_{si} with only the observation building (Condition 2) to that of a flat ground (Condition 1) is about 4, indicating that the site enhancement due to the observation building plays the most important role in the electric field measurement. When the building being struck is added (Condition 3), the simulated dE_{si} is about 10% less than that in Condition 2. We guess that as DPL1 develops downward, the increasing induced charges on the surface of the building being struck weaken the electric field change at the observation site. With the all 22 buildings (Condition 4) considered, the dE_{si} simulated is only about 3% less than that in Condition 3, suggesting that the surrounding buildings have little influence on the electric field measurement.

As Step 4 in section 3.3, with the observed dE_{ob}/dl in Figure 6b and the simulated dE_{si}/dl under Condition 4 in Figure 7, the leader channel line charge density and leader current versus the leader tip position of DPL1 are estimated based on Equations 6 and 7, as shown in Figures 8a and 8b, respectively.

The transferred leader line charge density (Figure 8a) for DPL1 has a minimum value of 0.4 mC/m and maximum value of 8.6 mC/m with a mean value of 2.3 mC/m. The transferred line charge density is about 3.2 mC/m when it begins at the height of about 1,860 m and quickly reaches the maximum of 8.6 mC/m when it goes down to the height of about 1,750 m and then decreases continuously from the maximum of 8.6 mC/m to the minimum of 0.4 mC/m as it goes down from about 1,750 to 300 m high. It should be mentioned that the line charge density estimated here is the charge transferred from the cloud into the leader corona sheath to balance the potential difference between the leader core and the ambient. The net charge left in the leader
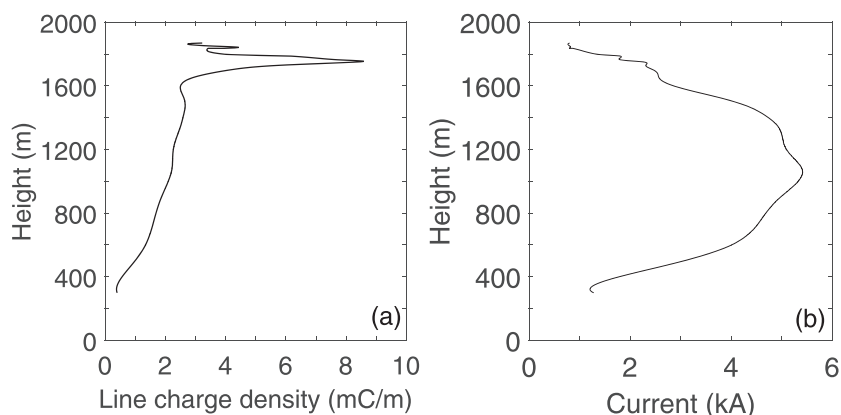
Figure 8. (a) The estimated transferred leader line charge density versus leader channel height and (b) the estimated leader current versus the leader tip height, for DPL1.
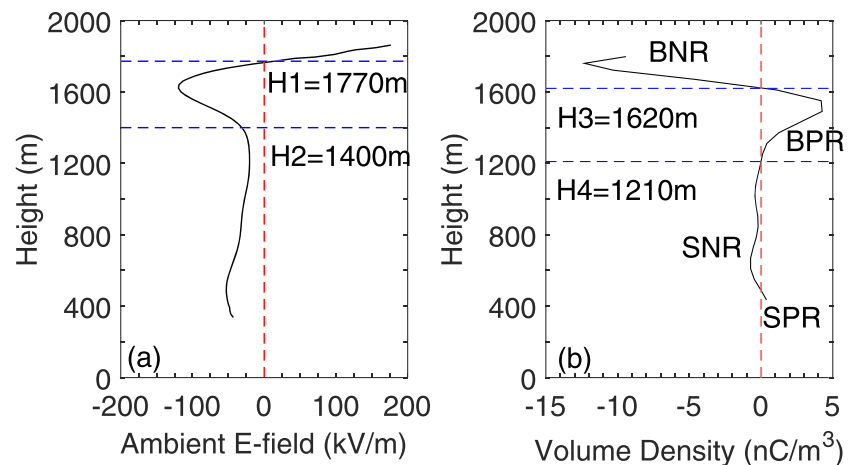
Figure 9. (a) Profile of the ambient electric field along the DPL1 path, estimated from the transferred leader line charge density in Figure 8a; (b) profile of the volume density of the space charge along the DPL1 path, estimated from the ambient electric field profile in (a). There are four obvious space charge regions: BNR—the upper big negative space charge region, BPR—the upper big positive space charge region, SNR—the lower small negative space charge region, and SPR—the lower small positive space charge region. H1–H4 are four special heights indicating the sign-reversing heights of the ambient electric field or the space charge profile.

corona sheath is this charge transferred plus the previously existed space charge along the leader channel path. The previously existed space charge may be positive or negative ones where or there.

The leader current (Figure 8b) for DPL1 is in the range of 0.7 to 5.4 kA with a mean value of 3.7 kA. It has the minimum value of 0.7 kA when at the height of about 1,860 m and reaches the maximum value of 5.4 kA when it goes down to the height of about 1,050 m and then decreases continuously to about 1.2 kA as it goes to the height of about 300 m.

As Step 5 in section 3.3, the transferred leader line charge density estimated is integrated and averaged for each 1 m element over a 20 m long channel segment, before it can be used to estimate the ambient electric field along the DPL1 path. Similarly, the ambient electric field profile estimated is integrated and averaged for each 20 m segment over a 60 m long channel length, before it can be used to get the volume density of the space charge along the DPL1 path. As a result, the length of the leader channel path for which the ambient electric field is estimated is a little bit shorter than that for the transferred leader charge density estimation and that for the space charge estimation is a little bit shorter than that for the ambient electric field estimation. The estimated profiles for the ambient electric field and the volume density of the space charge for DPL1 are shown in Figures 9a and 9b, respectively.

As shown in Figure 9a, the ambient electric field along the DPL1 path varies in the range of −120 to +180 kV/m. It starts with the maximum positive value of +180 kV/m at the height of about 1,860 m and decreases quickly to zero as it goes to about 1,770 m (H1) high. After that, it further decreases to a negative value and reaches the maximum negative value of −120 kV/m when it goes to about 1,620 m high and then reverses to increase quickly to about −30 kV/m when it goes to about 1,400 m (H2) high. When below 1,400 m, the ambient electric field fluctuates in a small range of −55 to −20 kV/m.

As shown in Figure 9b, the volume density of space charge along the DPL1 path varies in the range of −12.3 to +4.2 nC/m^3. There are two big space charge regions (BNR—big negative region and BPR—big positive region) in the upper part of DPL1 path and two small space charge regions (SNR—small negative region and SPR—small positive region) in the lower part of DPL1 path. The BNR is at the height of 1,620 (H3) to 1,800 m with a charge density of −12.3 to 0 nC/m^3, the BPR is at the height of 1,210 (H4) to 1,620 m with a charge density of 0 to +4.2 nC/m^3, the SNR is at the height of 490 to 1,210 m with a charge density of −0.7 to 0 nC/m^3, and the SPR is at the height of 440 to 490 m with a charge density of 0 to +0.37 nC/m^3. This suggests that DPL1 started in a region above the BNR (1,800 to 1,620 m) and went downward through the BPR (1,620 to 1,210 m), the SNR (1,210 to 490 m), and the SPR (490 to 400 m) in turn and finally attached to the grounded building.
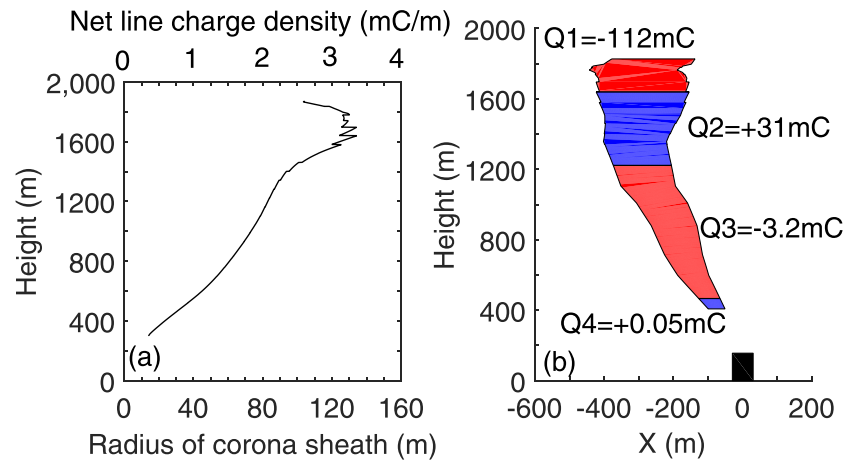
Figure 10. (a) The estimated leader channel corona sheath radius and net line charge density versus height for DPL1; (b) the estimated space charges within the channel corona sheath of DPL1 for the four space charge regions defined in Figure 9b: Q1 for BNR, Q2 for BPR, Q3 for SNR, and Q4 for SPR. The black block represents the building struck by DPL1.

According to Equation 15, assuming the radial electric field in the corona sheath is equal to the critical E field +500 kV/m required for positive streamer propagation, the equivalent corona sheath radius as well
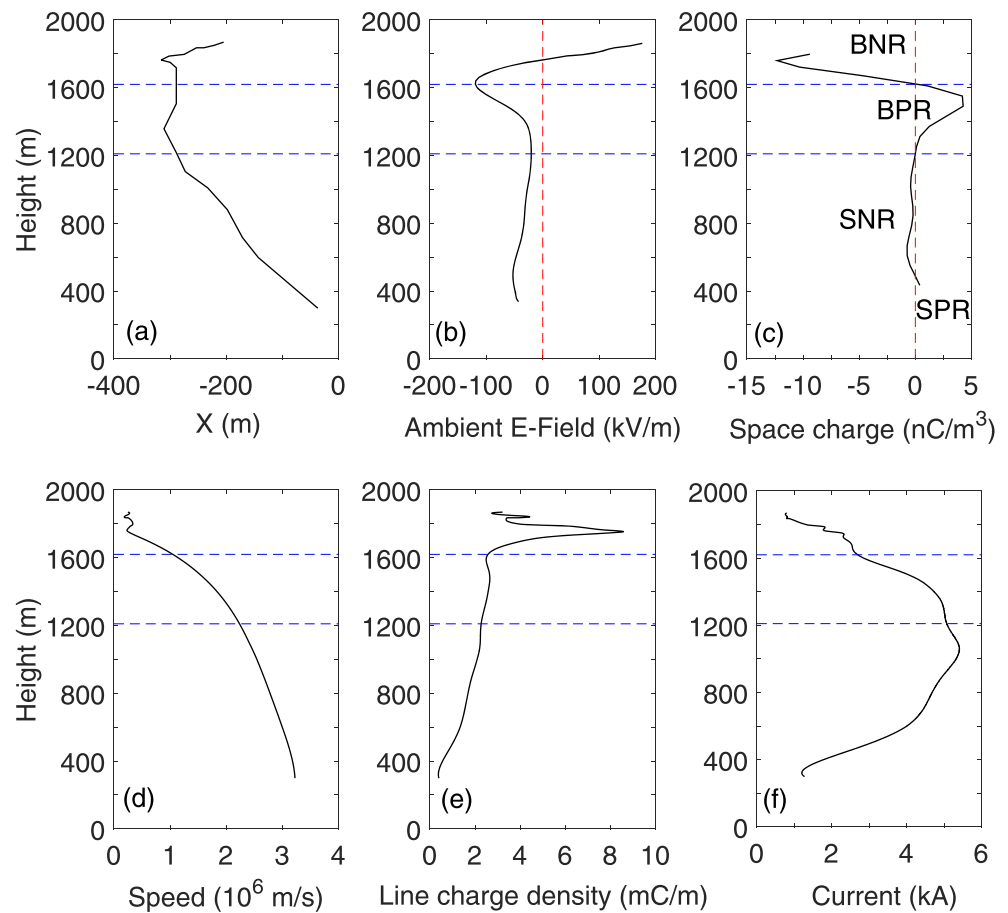
**Figure 11.** A comparison among leader parameters including (a) the leader channel path, (b) ambient electric field, (c) volume space charge density, (d) 2-D leader speed, (e) transferred leader channel line charge density, and (f) leader current, along the DPL1 channel path. The two blue dashed lines at the height of 1,620 and 1,210 m represent the boundaries between BPR, BNR, and SPR, respectively.
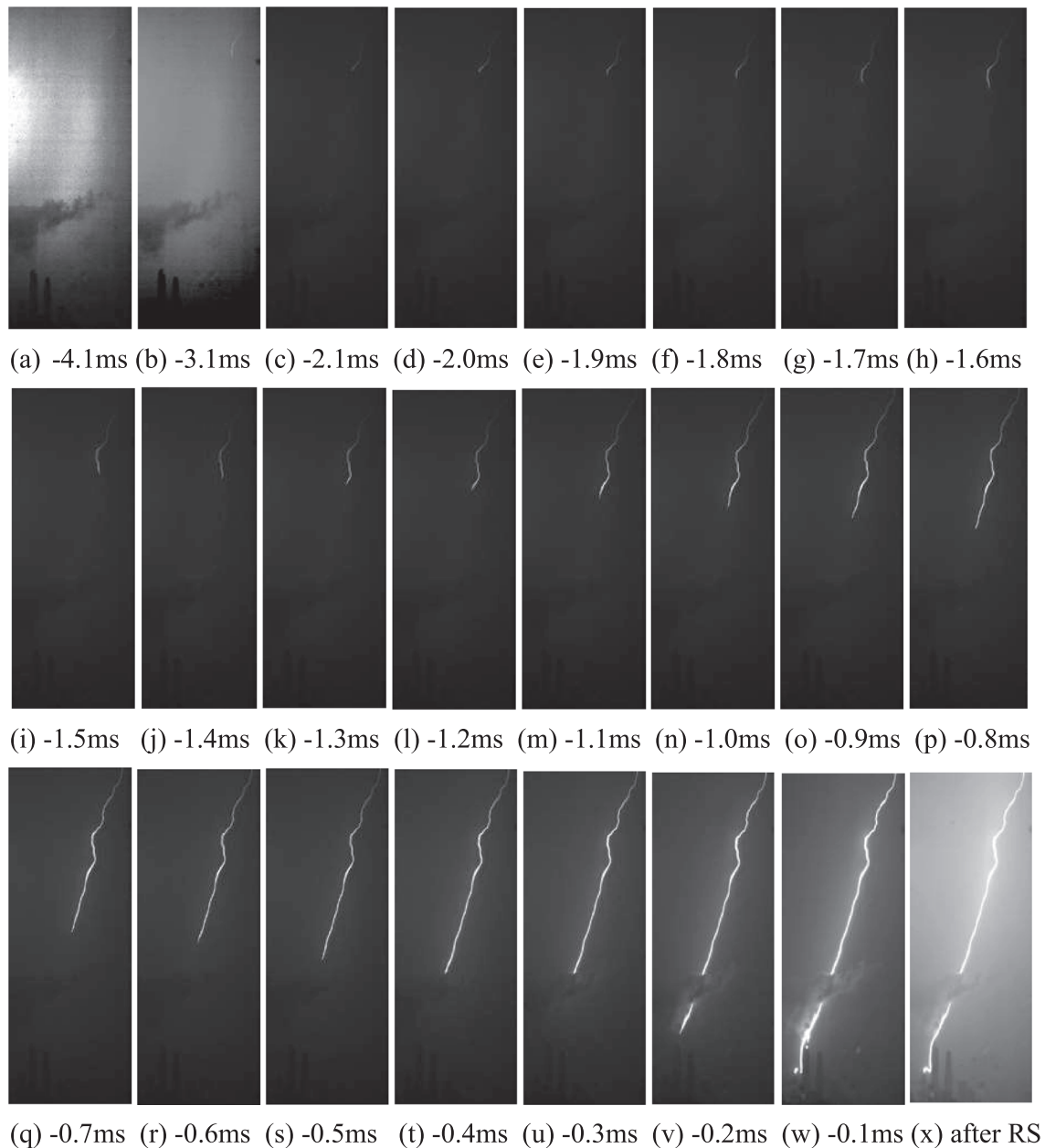
Figure 12. High-speed camera images of DPL2. Time 0 is set at the beginning of the return stroke. (a–w) Captured before the return stoke and (x) captured after that. A segment of the channel was shadowed by cloud in panel (u). Contrast enhancement is performed on (a) and (b) for easy reading of the channel. The extent of view of each panel is from about 100 to 3,100 m height above ground.

as the net leader line charge density of the DPL1 channel are estimated, as shown in Figure 10a. The corona sheath radius shows the same trend as the leader channel net line charge density of DPL1, ranging from 14 to 134 m. The net line charge density along the DPL1 channel has a range from 0.6 to 3.5 mC/m, which is smaller than the transferred line charge density shown in Figure 8a. The peak values of both the corona sheath radius and net line charge density appear at the height of about 1,650 m. This radius range of the corona sheath estimated here is a little bit wider than that of some previous studies (e.g., Edens et al., 2014; Gao et al., 2020). Furthermore, assuming the volume space charge density has a laterally uniform distribution in the corona sheath region, the amount of space charges in the four space charge regions (BNR, BPR, SNR, and SPR, defined in Figure 9b) existed in the corona sheath of DPL1 are estimated, as shown in Figure 10b, where Q1 = −112 mC is for BNR (upper red), Q2 = +31 mC for BPR (middle blue),
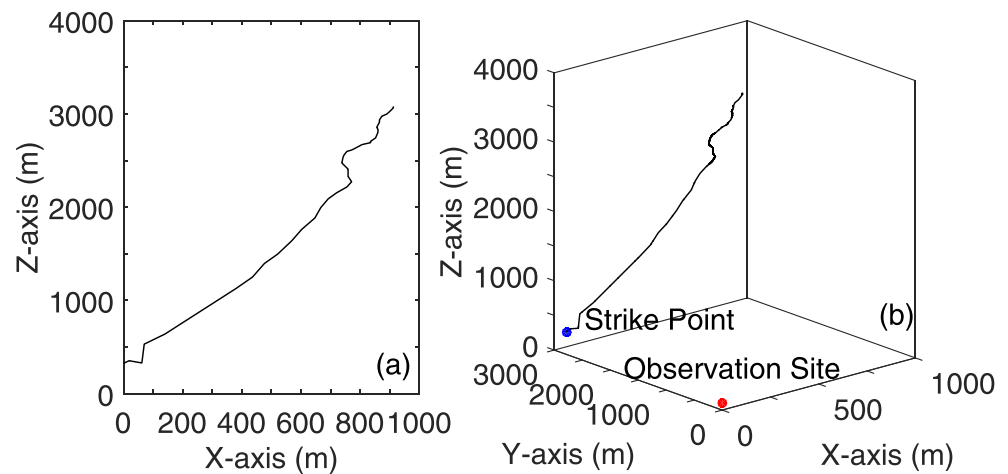
Figure 13. The 2-D channel rebuilt from HC-1 (a) and the channel in the 3-D coordinates in the simulation model (b) for DPL2. The horizontal distance from the observation site to the strike point is about 2,800 m.

Q3 = −3.2 mC for SNR (middle red), and Q4 = +0.05 mC for SPR (bottom blue), respectively. The black block represents the building struck by DPL1.

Figure 11 is a comparison between the leader channel path, ambient electric field, volume space charge density, leader speed, leader channel line charge density, and leader current for DPL1. It shows clearly that there are two big space charge regions (BNR and BPR) around 1,800 and 1,500 m high, respectively, which may reflect the electric structure of the cloud. The positive maximum of the ambient electric field, +180 kV/m, appears round 1,860 m high, which is the upper boundary of BNR. The negative maximum of the ambient electric field, −120 kV/m, appears around 1,620 m high, which is the boundary between BNR and BPR. The leader speed is the smallest of 10^5 m/s while the transferred leader line charge density is the maximum of 8 mC/m when within the BNR. As the leader goes into the BPR, the leader speed increases dramatically to above 10^6 m/s while the transferred leader line charge density shows a stable decreasing trend.

4.2. Case 2 (DPL2)

This was another DPL2 started cloud-to-ground positive lightning flash occurred at 15:56:00 on 13 August of 2015. Only one return stroke was recorded by the local lightning location network with a peak current of +163 kA.

Figure 12 shows a series of high-speed camera images of DPL2 taken at the observation site. The strike point of DPL2 was on the top of a building called Global Metropolitan Plaza. The height of the building was 326 m, and the horizontal distance from the building to the observation site was about 2,800 m. In Figure 12u, there is a segment of DPL2 channel shadowed by cloud so that the leader tip position cannot be obtained in this frame. A straight-line segment is used to replace this cloud-shadowed channel part in all following analysis. The rebuilt 2-D and 3-D channel for DLP2 are shown in Figures 13a and 13b, respectively.

From the 2-D channel images of DPL2, the 2-D speed of DPL2 is estimated, as shown in Figure 14a, where the blue line represents the raw data and the red line represents the curve-fitted speed. Since the channel tips were shadowed by cloud in Figures 12u and 12v, the corresponding channel segment are replaced with a straight line and the average speed for these two frames is estimated. As can be seen from the figure, the speed of DPL2 shows an obvious increasing trend with the time. The speed ranges from 1.7 to 46.9×10^5 m/s with a mean value of 7.5×10^5 m/s as the leader goes down from about 3,080 to 326 m high. Figure 14b shows the 2-D channel length versus time for DPL2, which is estimated based the curve-fitted 2-D speed shown in Figure 14a.

Figure 15a shows the electric field changes produced by DPL2 at the observation site. The two vertical dashed lines indicate the start (−4.1 ms) and end (−0.1 ms) times of the calculation. Time 0 is set at the beginning of the return stroke. The electric field change versus time is processed with the five-point moving method before it is converted to the channel length derivative of the electric field change versus time. The
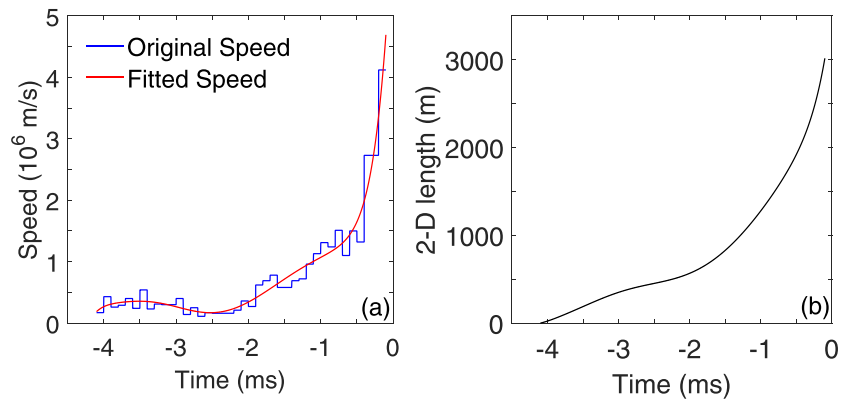
Figure 14. (a) The 2-D speed versus time for DPL2, the blue and red lines represent the observed and the curve-fitted speeds, respectively; (b) the 2-D channel length versus time for DPL1, obtained from the curve-fitted speed in (a). Time 0 is set at the beginning of the return stroke.

calculated dE_{ob}/dl versus time for DPL2 is shown in Figure 15b. There is a critical height 825 m that the polarity of dE_{ob}/dl is positive when above it and becomes negative when below it.

Similar to DPL1, simulations of the electric field change produced by a unit line charge density along the channel of DPL2 at the observation site are performed under the same four ground conditions as for DPL1. Figure 16 shows the channel length derivative of the simulated electric field change, dE_{si}/dl, for DPL2 under the four conditions. As can be seen from the figure, the electric fields simulated under the four conditions have the same trend that as the leader goes from about 3,000 m high downward, the dE_{si}/dl value firstly increases and reaches its maximum around 2,000 m high and then turns to decrease and has its sign reversed around 810 to 830 m high. This sign-reversing height for dE_{si}/dl is very close to the sign-revering height of 825 m in Figure 15b for dE_{ob}/dl, indicating that the simulation is reasonable compared with the observation. The little difference in the sign-reversing height between the observation and the simulation is due to partially the model simplification in the simulation and partially the data error in the observation.

The dE_{si}/dl value with all the 22 buildings considered (Condition 4) is about 3.4 to 3.6 times of that in Condition 1 (flat ground). The dE_{si}/dl value with only the observation building considered (Condition 2) is about 4 times of that in Condition 1, indicating that the observation building plays the most important role in the electric field measurement. The ratio of dE_{si}/dl with both the observation and struck buildings considered (Condition 3) to that in Condition 2 is about 0.9, indicating that the existence of the struck building weakens the electric field change at the observation site by 10%. The dE_{si}/dl value in Condition 4 is less than
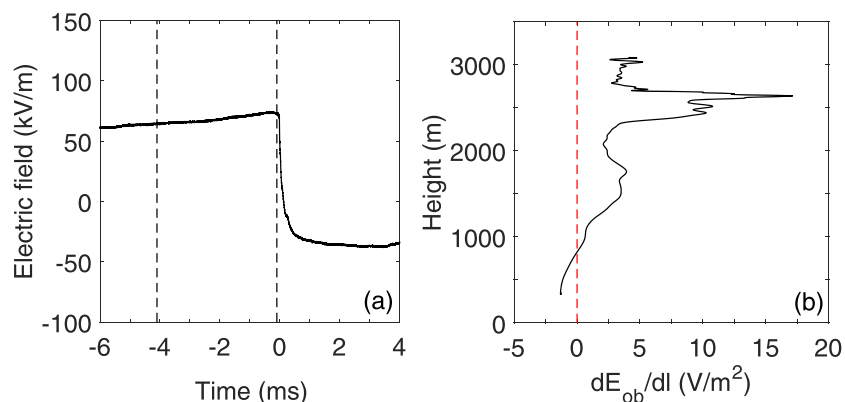
Figure 15. (a) The electric field change produced by DPL2, the two vertical dashed lines indicate the start (−4.1 ms) and end (−0.1 ms) times of the calculation; (b) the channel length-derivative of the electric field change, dE_{ob}/dl, versus height, calculated from the electric field change in (a) and the curve-fitted speed in Figure 14a for DPL2.
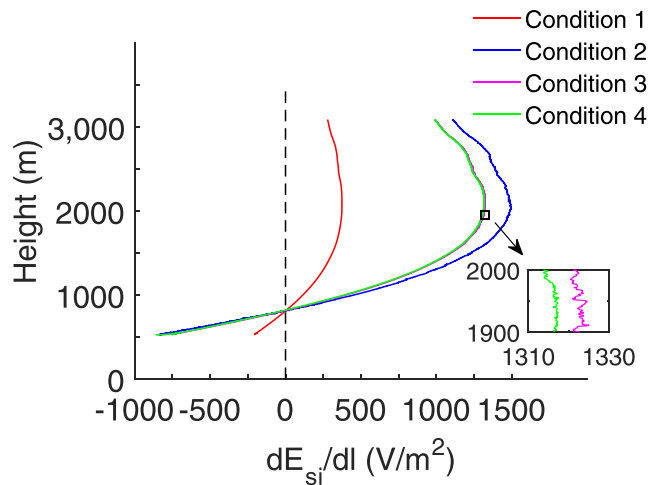
Figure 16. The simulated channel length derivative of the electric field change, dE_{si}/dl, versus height along the DPL2 channel with a unit (1 C/m) line charge density. Four curves represent the results under four ground conditions: red curve for Condition 1—a flat ground, blue curve for Condition 2—only the observation building on ground, purple curve for Condition 3—both the observation building and the building being struck by DPL2 on ground, and green curve for Condition 4—all the 22 buildings on ground. The subpanel is to show the difference between purple and green curves at the height of 1,900 to 2,000 m for easy reading.
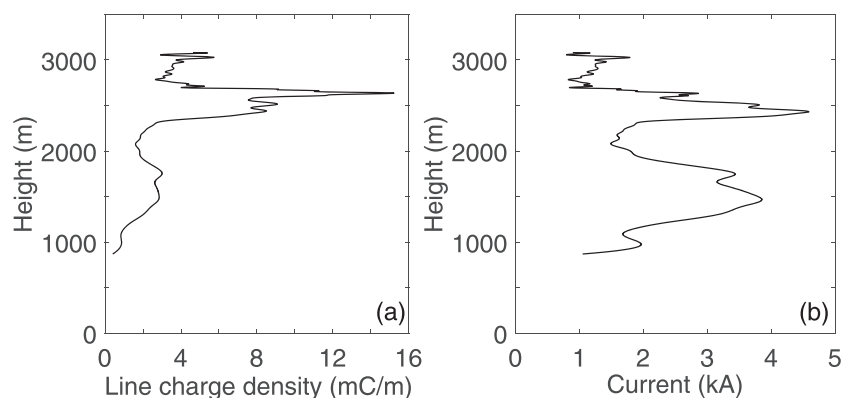
that in Condition 3 by about 3%, indicating that other 20 buildings have little influence on the electric field measurement.

As Step 4 in section 3.3, the transferred line charge density and leader current versus the leader tip position for DPL2 are estimated based on the $v(l)$ in Figure 14a, dE_{ob}/dl in Figure 15b and dE_{si}/dl under Condition 4 in Figure 16 with Equations 6 and 7, as shown in Figures 17a and 17b, respectively. To avoid extremum values of the transferred line charge density and leader current near the critical height, only the channel part above 870 m high is considered. The transferred line charge density of DPL2 has a value of about 4 mC/m when it is at the height of about 3,000 m and then increases quickly to the maximum value of 15.2 mC/m as it goes to the height of about 2,600 m. After that, it shows a generally decreasing trend and reaches its minimum value of 0.4 mC/m at the height of about 900 m, with a mean value of 3.4 mC/m. The leader current of DPL2 ranges in 0.7 to 4.6 kA with a mean value of 2.3 kA.

Shown in Figures 18a and 18b are the estimated ambient electric field and the space charge density along the path of DPL2, respectively. The ambient electric field for DPL2 fluctuates in a large range of −250 to +180 kV/m when it is above the height of 2,000 m and in a small range of −68 to +32 kV/m when it is below 2,000 m. The volume space charge density for DPL2 has three big space charge regions (BPR1 above 2,745 m, BNR above 2,340 m, and BPR2 above 1835 m) in the upper part of the leader channel and two small space charge regions (SNR and SPR) in the lower part of the leader channel below 1,835 m. The maximum volume densities for the three upper big space charge regions are +7.8 nC/m^3 (BPR1), −13.9 nC/m^3 (BNR), and +7.8 nC/m^3 (BPR2), respectively, and that for the two lower space charge regions are −2.1 nC/m^3 (SNR) and +0.9 nC/m^3 (SPR), respectively. This suggests that DPL2 started above the MPR1 (3,000 to 2,745 m) and went downward through BNR (2,745 to 2,340 m), BPR2 (2,340 to 1,835 m), SNR (1,835 to 1,250 m), and SPR (1,250 to 870 m) in turn and finally attached to the grounded building.

Based on Equation 15, given the radial electric field in the corona sheath is equal to +500 kV/m, the leader channel corona sheath radius and the leader channel net line charge density for DPL2 are estimated, as shown in Figure 19a. The corona sheath radius shows the same trend as the channel net line charge density of DPL2, ranging from 15 to 234 m. The net line charge density has a range from 0.4 to 5.8 mC/m, which is smaller than the transferred line charge density shown in Figure 17a. The peak values of both the corona sheath radius and net line charge density appear at the height of about 2,650 m. Assuming the volume space charge density has a laterally uniform distribution in the corona sheath, the amount of space charges existed

Figure 17. (a) The estimated transferred leader channel line charge density versus leader channel height and (b) the estimated leader current versus the leader tip height, for DPL2.
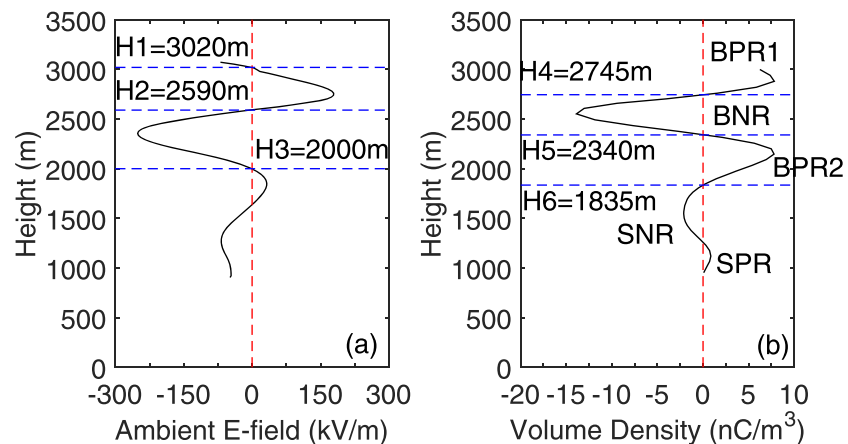
Figure 18. (a) Profile of the ambient electric field along the DPL2 path, estimated from the transferred leader channel line charge density in Figure 17a; (b) profile of the volume density of the space charge along the DPL2 path, estimated from the ambient electric field profile in (a). There are five obvious space charge regions: BPR1—upper big positive region 1, BNR—upper big negative region, BPR2—upper big positive region 2, SNR—lower small negative region, and SPR—lower small positive region. H1–H6 are six special heights indicating the sign-reversing heights of the ambient electric field or the space charge profile.

in the five space charge regions (BPR1, BNR, BPR2, SNR, and SPR in Figure 18b) within the corona sheath of DPL2 are estimated, as shown in Figure 19b, where $Q1 = +230$ mC is for BPR1 (upper blue), $Q2 = −460$ mC for BNR (upper red), $Q3 = +104$ mC for BPR2 (middle blue), $Q4 = −21$ mC for SNR (lower red), and $Q5 = +1.1$ mC for SPR (lower blue), respectively. The black block represents the building struck by DPL2.

Shown in Figure 20 is a comparison of leader parameters for DPL2, including the leader channel path, ambient electric field, volume density of space charge, leader speed, transferred leader channel line charge density, and leader current as a function of the leader tip height. The three dashed lines represent the boundaries between BPR1, BNR, BPR2, and SNR.

It can be seen that the ambient electric field has its maximum positive value ($+180$ kV/m) appeared at the boundary between BPR1 and BNR (2,745 m high), and its maximum negative value ($−250$ kV/m) appeared at the boundary between BNR and BPR2 (2,340 m high). The three big space charge regions (BPR1, BNR, and BPR2), which are supposed to be inside the cloud with the bottom of BPR2 (1,835 m high) as the cloud base, indicate that there can be strong variations of space charge distribution even within a small region of
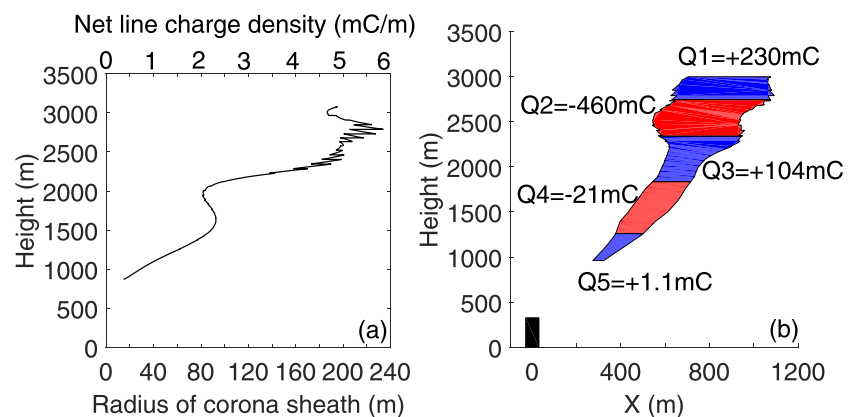
Figure 19. (a) The estimated leader channel corona sheath radius and leader channel net line charge density versus height for DPL2; (b) the estimated amount of space charges existed in the channel corona sheath of DPL1 for the five space charge regions in Figure 18b, where Q1–Q5 are the space charges for BPR1, BNR, BPR2, SNR, and SPR, respectively, and the black block represents the building struck by DPL2.
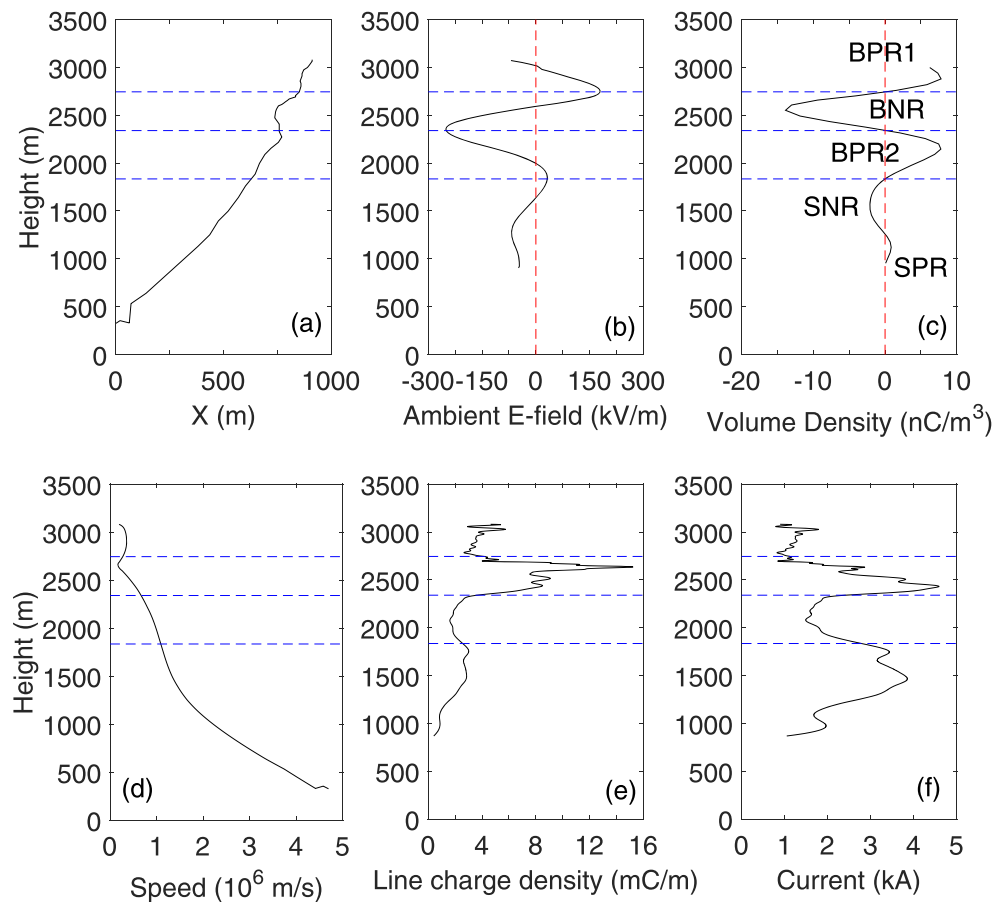
Figure 20. A comparison among leader parameters of the leader channel path (a), ambient electric field (b), volume space charge density (c), leader speed (d), transferred leader channel line charge density (e), and leader current (f), for DPL2. The three dashed lines represent the boundaries between MPR1, MNR, MPR2, and SNR at the heights of 2,745, 2,340, and 1,835 m, respectively.

the cloud. Both the leader current and transferred channel line charge density have their peaks appeared in BNR and then have a general decreasing trend as the leader goes out BNR toward ground.

It is also noted that the DPL2 channel has its direction slightly changed four times as the leader goes in and out the three main space charge regions, suggesting the distribution of in-cloud space charges may affect the leader propagation direction. The leader speed is the minimum of 1.7×10^5 m/s when it is in the BNR and increases continuously when it goes out the BNR toward ground with the maximum of 4.69×10^6 m/s appeared just before it strikes the building.

4.3. Error Analysis and Applicability of the Proposed Approach

There are many factors that may cause errors in the data analysis. First, since the observation site was in a metropolis with crowded buildings, various electromagnetic interferences could cause errors in the observed electric field. Second, the simplification of the crowded buildings and the cloud source position in the simulation model could cause inaccuracies in the simulation result. Third, the simplification of physical relations between leader parameters analyzed could cause errors in the estimation of the leader parameters. Fourth, while electrostatic modeling is used in the analysis, the electric field we measured may include some induction and radiation field components, which may add errors to the results. For the two cases in this study, the estimated percentage of the induction field to static field at the observation site is less than 0.2%, and that of the radiation field to static field is less than 0.005%.

In addition to above factors, the main error in the calculation may come from the 2-D channels and 2-D speeds of the two leaders. Since the 2-D leader speed is usually smaller than the 3-D speed, the use of the 2-D speed in the model could cause the leader charge density estimated being larger than the actual value. To get more accurate estimation of the leader charge density, 3-D information of the leader channel is necessary. In future, we expect to obtain more dual-station optical observations of lightning discharges to high-rise buildings so that the 3-D channel structure and 3-D speed of leaders can be reconstructed.

The proposed approach could be applied in situations where there is only one leader channel segment advancing during a given time period so that one can make sure that the electric field change obtained in the same time period is caused by that leader channel segment. In other words, this approach is suitable for estimating the leader channel charge density and leader current for an unbranched and smoothly moving leader process, including downward negative dart leaders with no stepwise movements.

5. Summary

In this study, we proposed a simulation-observation-combined approach for investigating the properties of various parameters associated with a downward leader striking a building based on optical and electric field observations made in metropolis area. The parameters investigated include the leader channel charge density and current as the leader goes downward and the ambient electric field and space charge previously existed along the leader channel path. With this approach, the spatial and temporal properties of two DPLs (DPL1 and DPL2) obtained in Guangzhou city of China were investigated. Main results are as follows:

1. The 2-D leader speed for both leaders shows a general increasing trend as the leader goes downward. The speed of DPL1 ranges in 1.8 to 32.3×10^5 m/s with a mean value of 11.1×10^5 m/s as the leader goes down from about 1,860 to 300 m high and that of DPL2 ranges in 1.7 to 46.9×10^5 m/s with a mean of 7.5×10^5 m/s as the leader goes down from about 3,080 to 326 m high.

2. The transferred leader channel line charge density for both leaders shows a similar trend that it has firstly a sharp increasing trend and then a decreasing trend as the leader goes downward. The transferred line charge density of DPL1 ranges in 0.4 to 8.6 mC/m with the peak appearing at 1,750 m high, and that of DPL2 ranges in 0.4 to 15.2 mC/m with the peak appearing at 2,635 m high. While the transferred line charge density for the upper part of the leader channel is higher, that for the lower part of the leader channel is comparable to most of previous results (e.g., Chen, Zheng, et al., 2013; Proctor, 1997; Shen et al., 2018). The leader current of DPL1 ranges in 0.7 to 5.4 kA with a mean of 3.7 kA and that of DPL2 ranges in 0.7 to 4.6 kA with a mean of 2.3 kA.

3. The ambient electric field for both leaders has an alternating polarity along the leader path. That for DPL1 has its positive maximum of +176 kV/m at 1,860 m high and its negative maximum of −120 kV/m at 1,620 m high and varies in the range of −55 to −20 kV/m when below 1,400 m. That for DPL2 has its positive maximum of +180 kV/m at 2,745 m high and its negative maximum of −250 kV/m at 2,340 m high and varies in the range of −68 to +32 kV/m when below 2,000 m. There is another negative ambient electric field region above the height of 3,020 m for DPL2, which is not seen for DPL1 probably due to the limited channel range observed. These results are well consistent with the magnitude of the electric field obtained with balloon sounding measurements and model simulations in literature (Chen, Gou, & Du, 2013; Mazur & Ruhnke, 1998; Schuur et al., 1991).

4. The space charge density for both leaders has also an alternating polarity along the leader path. For DPL1, there is a big negative space charge region (BNR) at 1,620 to 1,800 m high with a charge density of −12.3 to 0 nC/m^3 and a big positive space charge region (BPR) at 1,210 to 1,620 m high with a charge density of 0 to 4.2 nC/m^3, followed by two small negative/positive charge regions (SNR/SPR) below 1,210 m. For DPL2, there is a big positive charge region (BPR1) above 2,745 m with a charge density of 0 to +7.8 nC/m^3, a big negative charge region (BNR) at 2,340 to 2,745 m high with a charge density of −13.9 to 0 nC/m^3 and another big positive charge region (BPR2) at 1,835 to 2,340 m high with a charge density of 0 to +7.8 nC/m^3, followed by two small negative/positive charge regions (SNR/SPR) below 1,835 m. The big space charge regions may reflect the complexity of electric structure in the cloud, and the small ones may reflect the corona charge distribution in the space between the cloud and ground. Qi et al. (2018) inferred that the positive charge center was about 4 km high for a positive discharge in

Guangzhou. Some statistics showed that the thundercloud base in Guangzhou area was about 2 to 3 km or less. All these are comparable with the present results.

5. The equivalent radius of the leader channel corona sheath is ranged in 14 to 134 m for DPL1 and 15 to 234 m for DPL2, respectively. The net leader channel line charge density is ranged in 0.6 to 3.5 mC/m for DPL1 and 0.4 to 5.8 mC/m for DPL2, respectively. The amount of space charges existed in the corona sheath for the four space charge regions for DPL1 are −112 mC (BNR), +31 mC (BPR), −3.2 mC (SNR), and +0.05 mC (SPR), respectively, and that for the five charge regions for DPL2 are +230 mC (BPR1), −460 mC (BNR), +104 mC (BPR2), −21 mC (SNR), and +1.1 mC (SPR), respectively.

6. The simulation shows that the building where the electric field is measured has the dominant impacts on the electric field measurement. For the case in this study, the lightning-produced electric field on the roof of a 100 m high building is about 4 times of that on flat ground. The existence of the building struck by the lightning discharge makes the electric field about 10% less than without it. The existence of other surrounding buildings makes the electric field about 3% less than without them.

7. Comparisons between the leader development and the space charge distribution suggests that the space charge has certain impacts on the leader propagation direction. The DPL1 started above the BNR at 1,800 to 1,620 m high and went through the BPR at 1,620 to 1,210 m high and the SNR/SPR below 1,210 m in turn toward ground. The DPL2 started above the upper BPR1 at 3,000 to 2,745 m high and went through the BNR at 2,745 to 2,340 m high, the BPR2 at 2,340 to 1,835 m high and the SNR/SPR below 1,835 m in turn toward ground.

Data Availability Statement

Data used in this paper are available at website (http://doi.org/10.5281/zenodo.3723979).

References

Bazelyan, J. M., & Raizer, Y. P. (2000). *Lightning Physics and Lightning Protection*. Bristol, Philadelphia: Institute of Physics Publishing. https://doi.org/10.1887/0750304774

Becerra, M., & Cooray, V. (2006). A self-consistent upward leader propagation model. *Journal of Physics D: Applied Physics*, *39*(16), 3708–3715. https://doi.org/10.1088/0022-3727/39/16/028

Berger, K. (1975). Development and Properties of Positive Lightning Flashes at Mount San Salvadore, Paper Presented at Culham Conf.

Byrne, G., Few, A., & Weber, M. (1983). Altitude, thickness and charge concentration of charged regions of four thunderstorms during TRIP 1981 based upon in situ balloon electric field measurements. *Geophysical Research Letters*, *10*(1), 39–42. https://doi.org/10.1029/GL010i001p00039

Chan, M.-K., Chen, M., & Du, Y. (2018). A macroscopic physical model for self-initiated upward leaders from tall grounded objects and its application. *Atmospheric Research*, *200*, 13–24. https://doi.org/10.1016/j.atmosres.2017.09.012

Chen, M., Gou, X., & Du, Y. (2013). The effect of ground altitude on lightning striking distance based on a bi-directional leader model. *Atmospheric Research*, *125*, 76–83. https://doi.org/10.1016/j.atmosres.2012.08.019

Chen, M., Takagi, N., Watanabe, T., Wang, D., Kawasaki, Z. I., & Liu, X. (1999). Spatial and temporal properties of optical radiation produced by stepped leaders. *Journal of Geophysical Research*, *104*(D22), 27,573–27,584. https://doi.org/10.1029/1999JD900846

Chen, M., Zheng, D., Du, Y., & Zhang, Y. (2013). Evolution of line charge density of steadily-developing upward positive leaders in triggered lightning. *Journal of Geophysical Research: Atmospheres*, *118*, 4670–4678. https://doi.org/10.1002/jgrd.50446

Dellera, L., & Garbagnati, E. (1990). Lightning stroke simulation by means of the leader progression model. I. Description of the model and evaluation of exposure of free-standing structures. *IEEE Transactions on Power Delivery*, *5*(4), 2009–2022. https://doi.org/10.1109/61.103696

Edens, H. E., Eack, K. B., Rison, W., & Hunyady, S. J. (2014). Photographic observations of streamers and steps in a cloud-to-air negative leader. *Geophysical Research Letters*, *41*, 1336–1342. https://doi.org/10.1002/2013GL059180

Gao, Y., Chen, M., Qin, Z., Qiu, Z., Yang, Y., Du, Y. P., et al. (2020). The spatial evolution of upward positive stepped leaders initiated from a 356-m-tall tower in southern China. *Journal of Geophysical Research: Atmospheres*, *125*, e2019JD031508. https://doi.org/10.1029/2019JD031508

Gao, Y., Lu, W., Ma, Y., Chen, L., Zhang, Y., Yan, X., & Zhang, Y. (2014). Three-dimensional propagation characteristics of the upward connecting leaders in six negative tall-object flashes in Guangzhou. *Atmospheric Research*, *149*, 193–203. https://doi.org/10.1016/j.atmosres.2014.06.008

Gorin, B., Levitov, V., & Shkilev, A. (1976). Some Principles of Leader Discharge of Air Gaps with a Strong Non-uniform Field, Paper Presented at IEE Conf. Publ.

Idone, V. (1992). The luminous development of Florida triggered lightning. *Research Letters on Atmospheric Electricity*, *12*, 23–28.

Idone, V. P., Orville, R. E., & Henderson, R. W. (1984). Ground truth: A positive cloud-to-ground lightning flash. *Journal of Climate and Applied Meteorology*, *23*(7), 1148–1151. https://doi.org/10.1175/1520-0450(1984)023<1148:GTAPCT>2.0.CO;2

Iudin, D. I., Rakov, V. A., Mareev, E. A., Iudin, F. D., Syssoev, A. A., & Davydenko, S. S. (2017). Advanced numerical model of lightning development: Application to studying the role of LPCR in determining lightning type. *Journal of Geophysical Research: Atmospheres*, *122*, 6416–6430. https://doi.org/10.1002/2016JD026261

Kong, X., Qie, X., & Zhao, Y. (2008). Characteristics of downward leader in a positive cloud-to-ground lightning flash observed by high-speed video camera and electric field changes. *Geophysical Research Letters*, *35*, L05816. https://doi.org/10.1029/2007GL032764

Krehbiel, P. R. (1981). An Analysis of the Electric Field Change Produced by Lightning. PhD dissertation. University of Manchester Institute of Science and Technology, Manchester, England.

Krider, E., Weidman, C., & Noggle, R. C. (1977). The electric field produced by lightning leader steps. *Journal of Geophysical Research*, *82*(6), 951–960. https://doi.org/10.1029/JC082i006p00951

Lalande, P., Bondiou-Clergerie, A., Bacchiega, G., & Gallimberti, I. (2002). Observations and modeling of lightning leaders. *Comptes Rendus Physique*, *3*(10), 1375–1392. https://doi.org/10.1016/S1631-0705(02)01413-5

Le Boulch, M., & Plantier, T. (1990). The Meteorage thunderstorm monitoring system: A tool for new EMC protection strategies, paper presented at Proc. 20th Int. Conf. on Lightning Protection.

Les Renardieres Group (1977). Positive discharges in long air gaps at les Renardieres-1975 results and conclusions. *Electra*, *53*, 31–153.

Lu, W., Chen, L., Ma, Y., Rakov, V., Gao, Y., Zhang, Y., et al. (2013). Lightning attachment process involving connection of the downward negative leader to the lateral surface of the upward connecting leader. *Geophysical Research Letters*, *40*, 5531–5535. https://doi.org/10.1002/2013GL058060

Marshall, T. C., & Rust, W. D. (1991). Electric field soundings through thunderstorms. *Journal of Geophysical Research*, *96*(D12), 22,297–22,306. https://doi.org/10.1029/91JD02486

Marshall, T. C., & Rust, W. D. (1993). Two types of vertical electrical structures in stratiform precipitation regions of mesoscale convective systems. *Bulletin of the American Meteorological Society*, *74*(11), 2159–2170. https://doi.org/10.1175/1520-0477(1993)074<2159:TTOVES>2.0.CO;2

Maslowski, G., & Rakov, V. A. (2006). A study of the lightning channel corona sheath. *Journal of Geophysical Research*, *111*, D14110. https://doi.org/10.1029/2005JD006858

Maslowski, G., & Rakov, V. A. (2013). Review of recent developments in lightning channel corona sheath research. *Atmospheric Research*, *129*, 117–122. https://doi.org/10.1016/j.atmosres.2012.05.028

Mazur, V. (1989). Triggered lightning strikes to aircraft and natural intracloud discharges. *Journal of Geophysical Research*, *94*(D3), 3311–3325. https://doi.org/10.1029/JD094iD03p03311

Mazur, V., & Ruhnke, L. H. (1998). Model of electric charges in thunderstorms and associated lightning. *Journal of Geophysical Research*, *103*(D18), 23,299–23,308. https://doi.org/10.1029/98JD02120

Nakahori, K., Egawa, T., & Mitani, H. (1982). Characteristics of winter lighting currents in Hokuriku District. *IEEE Power Engineering Review*, *11*, 37–38. https://doi.org/10.1109/MPER.1982.5519845

Proctor, D. E. (1991). Regions where lightning flashes began. *Journal of Geophysical Research*, *96*(D3), 5099–5112. https://doi.org/10.1029/90JD02120

Proctor, D. E. (1997). Lightning flashes with high origins. *Journal of Geophysical Research*, *102*(D2), 1693–1706. https://doi.org/10.1029/96JD02635

Qi, Q., Lyu, W., Wu, B., Ma, Y., Chen, L., & Liu, H. (2018). Three-dimensional optical observations of an upward lightning triggered by positive cloud-to-ground lightning. *Atmospheric Research*, *214*, 275–283. https://doi.org/10.1016/j.atmosres.2018.08.003

Rakov, V. (1999). Lightning discharges triggered using rocket-and-wire techniques, paper presented at Recent research developments in geophysics (Vol. 2 (1999)).

Rakov, V. A., & Uman, M. A. (2005). *Lightning: Physics and effects*. New York: Cambridge University Press.

Rubenstein, M., Rachidi, F., Uman, M. A., Thottappillil, R., Rakov, V. A., & Nucci, C. A. (1995). Characterization of vertical electric fields 500 m and 30 m from triggered lightning. *Journal of Geophysical Research*, *100*(D5), 8863–8872. https://doi.org/10.1029/95JD00213

Saba, M. M., Cummins, K. L., Warner, T. A., Krider, E. P., Campos, L. Z., Ballarotti, M. G., et al. (2008). Positive leader characteristics from high-speed video observations. *Geophysical Research Letters*, *35*, L07802. https://doi.org/10.1029/2007GL033000

Schuur, T. J., Rust, W. D., Small, B. F., & Marshall, T. C. (1991). Electrical and kinematic structure of the stratiform precipitation region trailing an Oklahoma squall line. *Journal of the Atmospheric Sciences*, *48*(6), 825–842. https://doi.org/10.1175/1520-0469(1991)048<0825:EAKSOT>2.0.CO;2

Shen, Y., Chen, M., Du, Y., & Dong, W. (2018). Line charge densities and currents of downward negative leaders estimated from VHF images and VLF electric fields observed at close distances. *IEEE Transactions on Electromagnetic Compatibility*, *61*(5), 1507–1514.

Shepherd, T. R., Rust, W. D., & Marshall, T. C. (1996). Electric fields and charges near 0 C in stratiform clouds. *Monthly Weather Review*, *124*(5), 919–938. https://doi.org/10.1175/1520-0493(1996)124<0919:EFACNI>2.0.CO;2

Thomson, E. M., Uman, M. A., & Beasley, W. H. (1985). Speed and current for lightning stepped leaders near ground as determined from electric field records. *Journal of Geophysical Research*, *90*(D5), 8136–8142. https://doi.org/10.1029/JD090iD05p08136

Thottappillil, R., Rakov, V. A., & Uman, M. A. (1997). Distribution of charge along the lightning channel: Relation to remote electric and magnetic fields and to return-stroke models. *Journal of Geophysical Research*, *102*(D6), 6987–7006. https://doi.org/10.1029/96JD03344

Wada, A., Asakawa, A., Shindo, T., & Yokoyama, S. (2003). Leader and Return Stroke Speed of Upward-Initiated Lightning, paper presented at Proc. of 10th International Conference on Atmospheric Electricity.

Wang, D., Watanabe, T., & Takagi, N. (2011). A High Speed Optical Imaging System for Studying Lightning Attachment Process, paper presented at 2011 7th Asia-Pacific international conference on lightning, IEEE.

Xu, Y., & Chen, M. (2013). A 3-D self-organized leader propagation model and its engineering approximation for lightning protection analysis. *IEEE Transactions on Power Delivery*, *28*(4), 2342–2355. https://doi.org/10.1109/TPWRD.2013.2263846